Influence of substrate, process conditions, and post-annealing temperature on the properties of ZnO thin films grown by SILAR method

Bijoy Chandra Ghos[1,2†], Syed Farid Uddin Farhad[1†,*], Md Abdul Majed Patwary[2,3], Shanta Majumder[1**,2], Md. Alauddin Hossain[2], Nazmul Islam Tanvir[1], Mohammad Atiqur Rahman[2], Tooru Tanaka[3], and Qixin Guo[3]**

[1]Energy Conversion and Storage Research Section, Industrial Physics Division (IPD), BCSIR Labs, Dhaka 1205, Bangladesh Council of Scientific and Industrial Research (BCSIR), Bangladesh; nazmul.tanvir88@gmail.com (N.I.T.)

[2]Physical Chemistry Research Laboratory, Department of Chemistry, Comilla University, Cumilla-3506, Bangladesh; bijoycou037@gmail.com (B.C.G.), alauddincou21@gmail.com(M.A.H.), shantamajumder4@gmail.com (S.M.), mamajedp@gmail.com (M.A.M.P.), atiqche31@yahoo.com

(M.A.R.)

[3]Department of Electrical and Electronic Engineering, Saga University, Honjo, Saga 840-8502, Japan

ttanaka@cc.saga-u.ac.jp (T.T), guoq@cc.saga-u.ac.jp (Q.G)

†Contributed equally to this work

**Student during postgraduate research in IPD, BCSIR.

*Correspondence: sf1878@my.bristol.ac.uk (S.F.U. Farhad)

ABSTRACT: Here we report the effect of substrate, sonication process, and post-annealing on the structural, morphological, and optical properties of ZnO thin films grown in the presence of isopropyl alcohol (IPA) at temperature 30 – 65 ℃ by successive ionic layer adsorption and reaction (SILAR) method on both soda lime glass (SLG) and Cu foil. The X-ray diffraction (XRD) patterns confirmed the preferential growth thin films along (002) and (101) plane of wurtzite ZnO structure while grown on SLG and Cu foil substrate respectively. Both XRD and Raman spectra confirmed the ZnO and Cu-oxide phases of the deposited films. Scanning electron microscope (SEM) image of the deposited films shows compact and

uniformly distributed grains for samples grown without sonication while using IPA at temperature 50 and 65 ℃. The post-annealing treatment improves the crystallinity of the films, further evident by XRD and transmission and reflection results. The estimated optical bandgaps are in the range of 3.37-3.48 eV for as-grown samples. Results revealed that high-quality ZnO thin films could be grown without sonication using IPA dispersant at 50 ℃, which is much lower than the reported results using the SILAR method. This study suggests that in the presence of IPA, the SLG substrate results in better c-axis oriented ZnO thin films than that of DI water, ethylene glycol, propylene glycol at the optimum temperature of 50 ℃. Air-annealing of the samples grown on Cu foils induced the formation of Cu_xO/ZnO junctions which is evident from the characteristic I-V curve including the structural and optical data.

Keywords: ZnO thin films, SILAR, IPA dispersant, copper oxide, Post-annealing, Cu_xO/ZnO diode

1. INTRODUCTION

ZnO is amongst the most widely used n-type metal oxide semiconductor materials because of its unique structural, optical and electrical properties in conjugation with cheap, non-toxic nature, and natural abundance. [1-3] It has distinctive optoelectronic and physical properties such as tunable direct wide bandgap of about 3.37 eV, high transparency (>80 %) in the visible region, and large exciton binding energy (60 meV) at room temperature, [4-12] optimum refractive index (n ≈ 2.0), notable electron mobility (as large as 155 $cm^2/V.s$).[13-15] Moreover, ZnO are chemically and thermodynamically stable and basically crystallizes in the hexagonal wurtzite structure.[16] All the above unique features make ZnO a suitable material for diverse applications including anti-reflective coating (ARC), thin film solar cells[17] and transparent conductive oxide for flat panel displays,[18,19] photodiodes, [20] gas sensors, [21,22] light emitting diodes,[23] surface acoustic waves,[24]

protective surface coatings,[25] piezoelectric transducers[26] etc. These potential applications have boosted research related to the development of better quality ZnO thin films over the span of ongoing decades.

Both physical and chemical methods have been used for the synthesis of ZnO thin films for instances, successive ionic layer adsorption and reaction (SILAR),[27,28] chemical bath deposition (CBD),[29] pulsed laser deposition (PLD),[30] RF magnetron sputtering,[31] metal organic chemical vapour deposition (MOCVD),[32] sol-gel derived dip coating,[33] spray pyrolysis,[16] hydrothermal,[34] molecular beam epitaxy,[35] drop casting,[36] water oxidation[37], electrodeposition[38] , atomic layer deposition[39], and different sol-gel derived spin coating[40] techniques etc. Some of the above mentioned deposition techniques have disadvantages such as usage of surfactants, high processing temperatures, hazardous chemicals, highly-priced and sophisticated instruments.[39] Specifically, the major demerits of Atomic Layer Deposition (ALD) is the rate of speed and deposition of fractional monolayer per cycle as well as the chance of staying residues from precursor solution to the chamber [41]. Similarly, the main cons of electrodeposition method is the lower rate of film deposition and the requirement of conducting substrates. Moreover, controlling thickness with current density is a challenging matter.[42] However, among the chemical route synthesis techniques, SILAR is one of the simplest and economically favorable chemical methods because it produces durable and adherent thin films comparatively at low processing temperatures and it does not require any sophisticated and modern instrument.[40,43] Furthermore, this technique allows bulk region deposition on various kind of insulating, semiconducting, as well as conducting metallic substrates such as soda lime glass (SLG) microscopy slides, fluorine doped tin oxides (FTO), and Cu foil substrates [16,44,45] just to name of a few. The deposition technique relies on wide range of processing parameters such as bath temperature, solution pH, complexing and dispersant agents, and rinsing procedures [46-50] etc. to tailor physical properties of the material under investigation.

To our best knowledge, only a few reports have been published so far regarding the deposition of

ZnO thin films on Cu foil. Raidou et al.[51] have grown ZnO thin films on three kinds of substrates such as Cu, Si, and glass by the SILAR method. They have showed that the structure of the film depends strongly on the nature of the substrate, for instance, ZnO particles deposited on Cu substrate formed hexagonal structure whereas spindles shape was formed on the Si substrate and for glass substrate the film was in the form of small flowers and prisms.[51]

Gao et al.[28] first reported ZnO thin films deposition by incorporating an ultrasonic rinsing step in the SILAR method. Subsequently, Shei et al. improved the process and investigated the effects of deionized water (DI), ethylene glycol, and propylene glycol between the rinsing steps as well as rinsing temperature on the structural and optical properties of ZnO thin films. In those cases, ethylene glycol may impose environmental risks.[5] They also reported that higher growth temperature is necessary to produce highly c-axis oriented ZnO thin films when using ethylene glycol and propylene glycol during the rinsing processes.[5,52,53] To address above issues, this study aims to investigate the influence of sonication, usage of isopropyl alcohol (IPA) dispersant, and thereafter post-annealing effect on the structural, morphological, and optical properties of SILAR deposited ZnO thin films on SLG and Cu foil substrates. Cu foils were chosen mainly to investigate the copper oxide forming conditions near the ZnO nucleation cite, as well as the formation of Cu_2O/ZnO or CuO/ZnO junctions depending on IPA and post-annealing temperature. The use of IPA showed a strong effect as dispersing agent over other conventional dispersants and the post-annealing of SILAR samples on Cu foil was found to be beneficial for making Cu_xO/ZnO (x = 1, 2) heterojunction. These experimental results are presented and discussed below.

2. RESULTS AND DISCUSSION

2.1. Structural Characterization

The phase and crystal structure of both as-deposited and annealed samples were analyzed from the XRD patterns in the range of 2θ = 25-45° shown in Figure 1. The deposited samples grown on SLG exhibited

three intense peaks at 2θ≈31.74°, 34.40° and 36.21° which could be assigned respectively to (100), (002) and (101) planes of ZnO with hexagonal wurtzite structure.[36] No diffraction peaks of $Zn(OH)_2$ were discernible in the XRD patterns (see Figure 1a). XRD patterns of samples grown on Cu-foil including pristine and annealed Cu-foil are shown in Figure 1b for comparison purpose. The Cu-foil air annealed at 250 ^{0}C for 1 h exhibits a broad peak near 2θ = 36 deg. suggesting the formation of CuxO phase atop the Cu surface. Notice also that thin films deposited on Cu foil exhibited same crystallographic nature of ZnO similar to SLG thin films while grown without sonication steps (cf. C4, C5, C6) and no discernible ZnO peaks (XRD patterns not shown here) while grown with sonication steps included in the SILAR process (cf. C1, C2, and C3). However, for all all-post-annealed thin films on Cu-foil exhibited preferable orientation along the (101) plane of ZnO, where the diffraction peak at 2θ ≈ 43.5° corresponds to the Cu (111) plane arising from the underlying substrate (see Figure 1b). Strikingly, all of the Cu foil samples produced Cu_xO/ZnO (x =1, 2) structure after post-annealing at 250 ℃ irrespective of the growth temperature with IPA and sonication process (see top panels in Figure 1b). This may be due to the oxidation of Cu foil substrate as can be seen from both XRD and Raman spectra depicted in Figure 1b and Figure 2b. Above results suggest the formation of Cu-oxide/ZnO heterojunction depend only on the post-annealing but not on the sonication process and neither on the IPA dispersant used. Thus, the post-annealing is beneficial for the formation of Cu_xO/ZnO heterojunctions.[16,51,54] The strong diffraction peak along (002) plane for the as-deposited G5(IPA50) and G6(IPA65) samples signifies highly c-axis oriented ZnO films[36] which was absent for G4(IPA30) samples, suggesting that temperature of IPA promotes crystallinity of the as-deposited ZnO film. The intensity of the concerned diffraction peak was seen to increase further after post-annealing. Therefore, increasing the IPA temperature and post-annealing improved the crystallinity of the deposited thin films.[36,52] The same trend was also observed for samples deposited on Cu foil. In both cases, SILAR process produced better crystalline thin films without sonication steps and the good quality films could be

formed using IPA with a minimum of 50 ℃ evident from Figure 1. Shei *et al.*[5,52] have reported no film growth below 75 ℃ and 95 ℃ respectively by using ethylene glycol and propylene glycol.

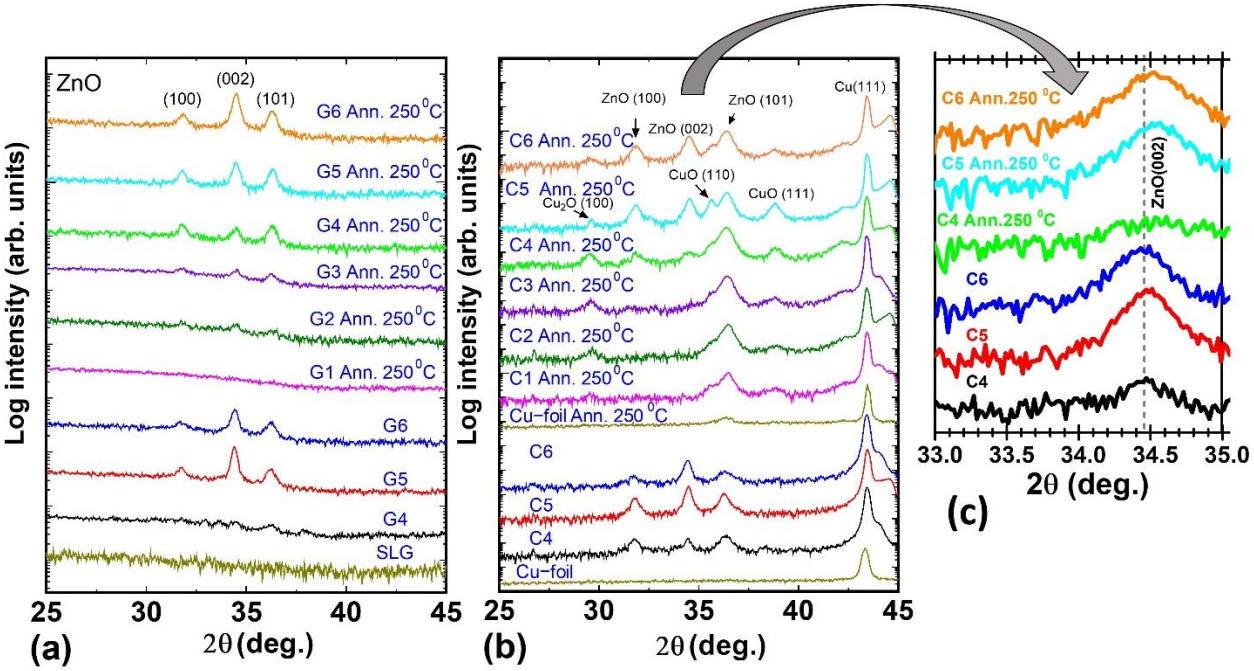

Figure 1. XRD patterns of both as-made and post-annealed samples grown on **(a)** SLG and **(b)** Cu foil. The XRD patterns of blank SLG and Cu-foil (pristine and air annealed at 250 ^{0}C for 1 h) substrates are also included for comparison purposes. The diffraction peaks of corresponding materials are shown by arrow sign for clarity. A zoomed part of the XRD patterns near ZnO (002) peak for sonication less SILAR samples grown on Cu foils is shown in (c).

It is inferred from Figure 1a that highly textured films can be prepared for samples G5(IPA50) and G6(IPA65) without sonication steps. This may be due to the fact that IPA acts as a better dispersant compared to ethylene glycol, propylene glycol and DI water reported in refs.[5,52,53] and results in depositing better quality ZnO thin films.

The important structural parameters and mean crystallite sizes (D) of samples grown without sonication steps were calculated by using Scherrer equation[55] to the 002 diffraction peak of ZnO and summarized in Table 1:

$$D = \frac{k\lambda}{\beta cos\theta} \quad (1)$$

Where, λ= wavelength of X-ray (0.15406 nm for CuKα radiation source), k= constant which is 0.94, β = Full width at half maxima (FWHM), θ= Diffraction angle.

The micro-strain (ε) due to the peak broadening is distributed within the material and it can be estimated using Wilson formula [56] :

$$\varepsilon = \beta / 4\tan\theta \quad (2)$$

Table 1. Mean crystallite size and lattice strain of as-made and annealed samples deposited on SLG and Cu-foil using IPA at different temperatures.

Sample	2θ (deg.)	FWHM (deg.)	Crystallite size ± 0.5 (nm)	Micro-strain (ε) $\times 10^{-3}$
G4(IPA30)	34.39	0.66	13	9.3
G4 Ann. 250 ℃	34.47	0.42	21	5.9
G5(IPA50)	34.41	0.34	26	4.8
G5 Ann. 250 ℃	34.48	0.43	20	6.0
G6(IPA65)	34.42	0.36	24	5.1
G6 Ann. 250 ℃	34.49	0.38	23	5.3
C4(IPA30)	34.45	0.44	20	6.2
C4 Ann. 250 ℃	34.67	1.07	8	15.0
C5(IPA50)	34.48	0.42	21	5.9
C5 Ann. 250 ℃	34.55	0.52	17	7.3
C6(IPA50)	34.43	0.56	16	7.9
C6 Ann. 250 ℃	34.52	0.63	14	8.8

It is evident from the Table 1 that the mean crystallite sizes were 13-26 nm and 20-23 nm respectively for as-deposited and annealed samples grown on SLG. The crystallite size increases and the micro-strain

decreases with post-annealing at 250 ℃ (G4 Ann.250 ℃ and G6 Ann.250 ℃) which signifies the improvement of the crystallinity[5] of the films (see also Figure 1a). On the other hand, in case of samples grown on Cu-foil, the mean crystallite sizes were estimated to be 16-21 nm, and intriguingly, reduced crystallite size was observed for post-annealed samples as evident from the ZnO (002) peak broadening shown in Figure 1c. The samples deposited at 50 ℃ without sonication exhibited the highest crystallinity (D = 26 nm for G5 and 21 nm for C5) and minimum micro-strain among all samples with (002) preferential growth. Therefore, these observations indicate the optimum temperature in presence of IPA should be 50 ℃ for growing better quality c-axis oriented ZnO thin films without sonication steps. Notice also that in the case of Cu-foil samples, ZnO(002) peaks are shifted to the higher Bragg angle for post-annealed samples compared to as-made samples (see dotted vertical line in Figure 1c), this is presumably due to strain-stress effect induced by the formation of CuxO underneath the ZnO film (see ref.[40] and refs. therein).

2.2. Raman Analysis

Room temperature Raman measurements of samples deposited on both SLG and Cu foil were carried out to identify the phase purity of Zn- and Cu-oxides as well as to investigate the effect of processing conditions on their crystalline structure. Raman spectroscopy is an effective tool to analyze the small changes as the vibrational signals are very sensitive to the local environment of the molecule, crystal structure, chemical bond, etc.[57] The Raman spectra of the samples deposited on both SLG and Cu foil are shown in Figure 2a and Figure 2b respectively.

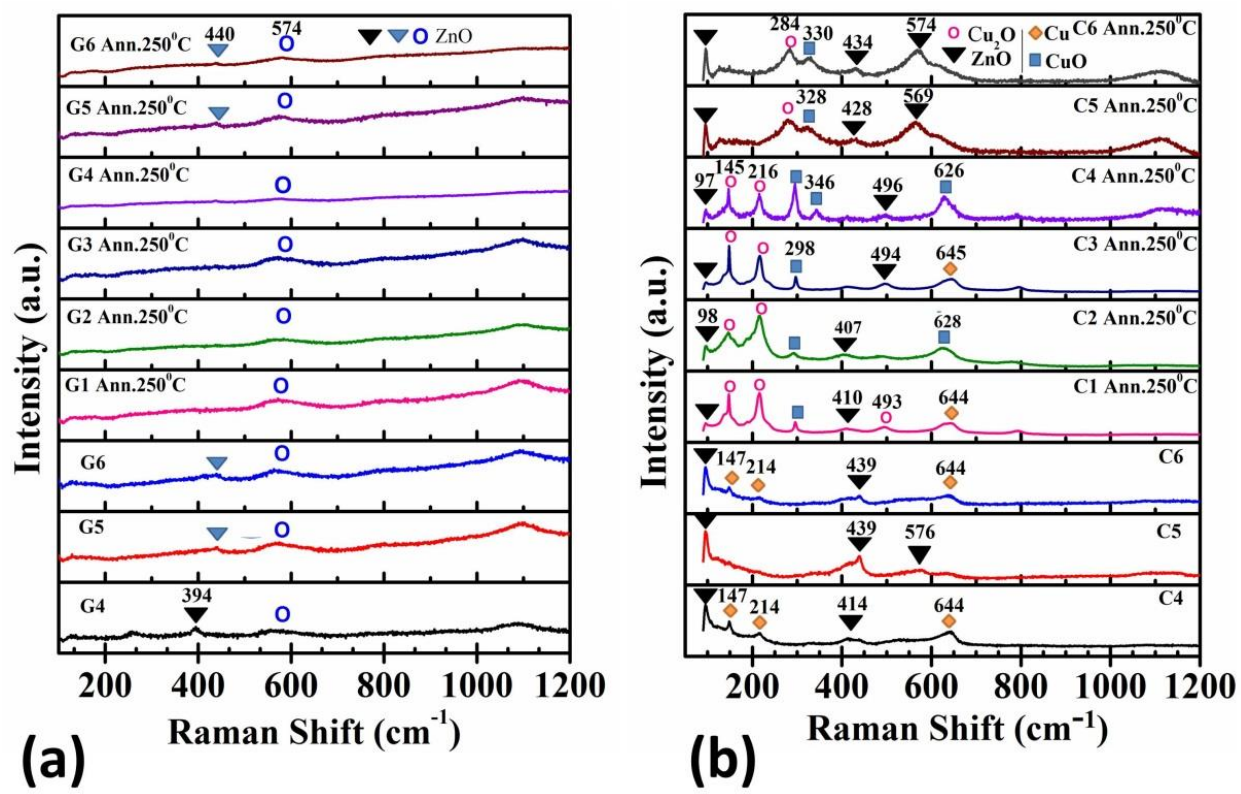

Figure 2. Raman spectra of the samples grown on **(a)** SLG and **(b)** Cu foil. The reference Raman shift values are indicated by different symbols in the figure.

It is clear from Figure 2a that the post-annealing exhibited a broad Raman signal approximately at 574 cm^{-1} which could be attributed to ZnO[58] for samples G1 Ann. 250 ℃ and G2 Ann. 250 ℃ for which XRD peaks were not clear in Figure 1a. In contrast, the samples G5(IPA50) and G6(IPA65) (without sonication) showed two distinguishable peaks centering at ~440 and ~574 cm^{-1} which have been attributed to highly crystalline c-axis oriented ZnO films due to a decrease of defects in the interior of the crystal.[58]

In Figure 2b, the films on Cu foil show Raman peaks centering at 97, 98, 405, 407, 410, 428, 434, 494, 496, 569 and 574cm^{-1} correspond to ZnO phase. Moreover, the Raman signals for copper oxide (Cu_2O+CuO) mixture phases were evidenced for all annealed samples (C1 Ann. 250 ℃ to C6 Ann. 250 ℃). The Raman peaks of ZnO/Cu foil are seen to be slightly blue shifted compared to those of ZnO/SLG due to strain induced by

copper oxide phase between Cu foil and ZnO layer. This is also consistent with the XRD observations shown in Figure 1c. In addition, peaks at around 147, 214, 644cm^{-1} appeared for samples grown on the Cu foil. The additional phonon modes appeared close to 145, 216, 284, 493 cm^{-1} can be attributed to Cu_2O phase and those close to 298, 330, 346, 626 cm^{-1} can be attributed to the CuO phase.[57-66] These observations indicate the possibility of the facile Cu_xO/ZnO (x =1,2) formation by post-annealing at a temperature as low as 250 ℃, and are also in consistent with the observed XRD pattern shown in Figure 1b. From both XRD and Raman analyses, it can be concluded that for depositing single phase highly crystalline c-axis oriented ZnO films, it may be better to use sonication step(s) less SILAR process irrespective of substrate type and do post-annealing at 250 ℃ for 1h results for facile formation of Cu-oxide/ZnO heterojunction while Cu foil is used.

2.3. Morphological characterization

Figure 3 compares the surface morphologies of thin films grown on both SLG and Cu foil. From Figure 3a and Figure 3d, it is clearly seen that the samples deposited using IPA at 30 ℃ (labeled as IPA30) exhibited cotton-like amorphous morphology (see also XRD patterns in Figure 1). In contrast, compact and uniformly distributed spherical grains were observed both for pristine IPA50 and IPA65 samples. Thus, at relatively high temperatures good quality coherent films are produced as it provides sufficient energy for complete conversion of $Zn(OH)_2$ to ZnO.[5] The grain sizes of the films grown on SLG were slightly larger (~260-300 nm) than the grain size of those grown on Cu foil (~200-230 nm) further indicating better quality films corroborating the XRD results. Some over grown clusters for Cu foil-samples can be seen which might be detrimental for device applications. Thus, the film quality is not affected only by the temperature of the IPA but also the types of substrate. Previous studies reported that relatively higher temperature (≥ 95 ℃) was required to decrease agglomeration for ethylene glycol and propylene glycol used as dispersing agent.[5,52] Since isopropyl alcohol is a monohydric alcohol, it forms only inter-molecular hydrogen bond [67]

and affects the deposition process, free from releasing thermal energy due to the breaking of intra-molecular H-bonding. Consequently, $Zn(OH)_2$ species are easily removed through H-bonding which are loosely adsorbed on the ZnO surface. This property makes IPA to act as a better dispersant than ethylene glycol and propylene glycol at relatively low temperatures.[68] Intriguingly, the IPA50 sample grown without sonication exhibited a coherent microstructural morphology together with appreciable crystallite size (D = 26 nm) and optical bandgap (Eg = 3.37 eV). These observations assert that the surface morphologies can be controlled by controlling the IPA temperature and by selecting a suitable substrate.

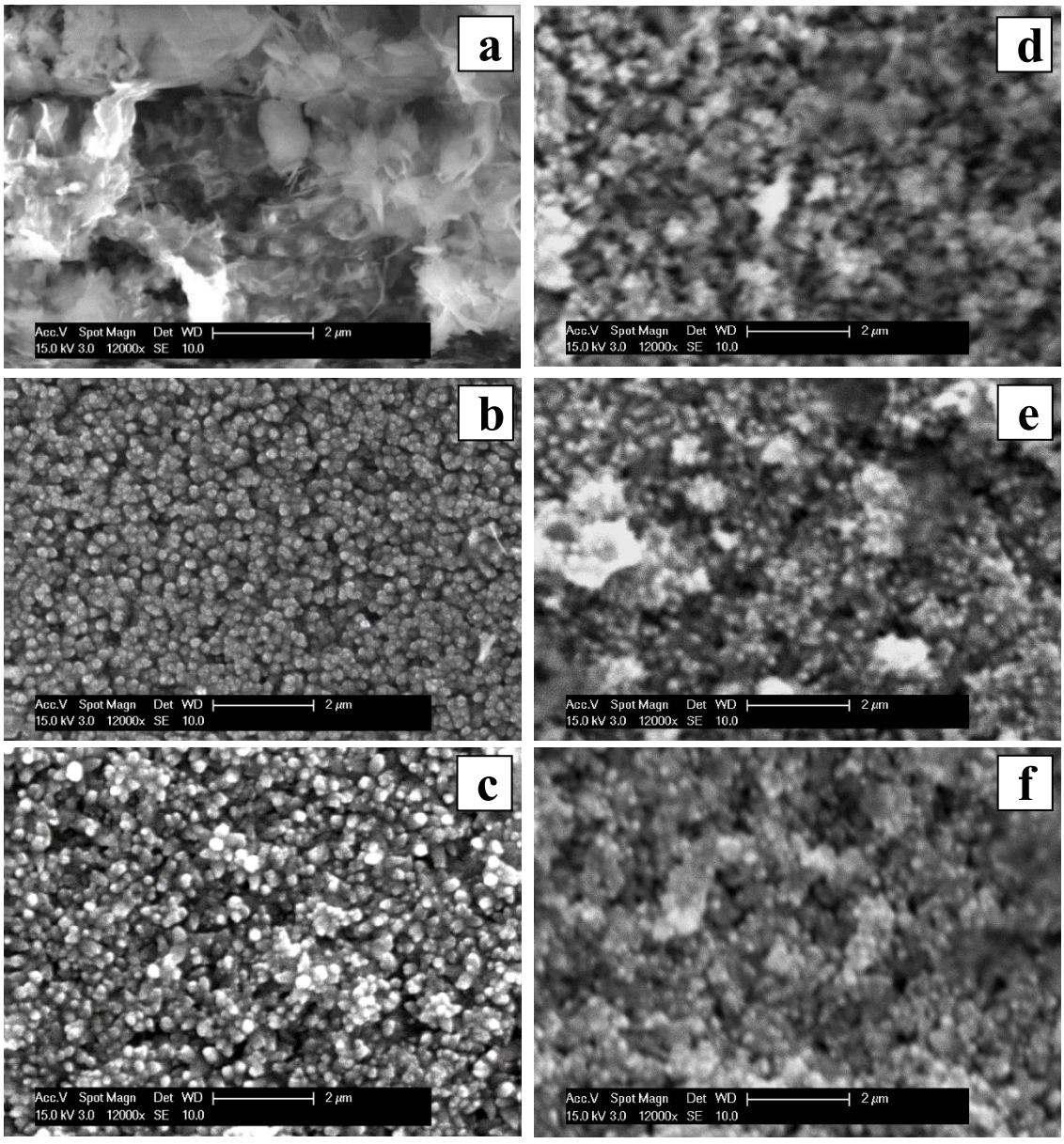

Figure 3. SEM micrographs of the samples deposited using IPA dispersant at various temperatures on SLG **(a)** G4(30 ℃), **(b)** G5(50 ℃),**(c)** G6(65 ℃); and on Cu foil **(d)** C4(30 ℃), **(e)** C5(50 ℃), **(f)** C6 (65 ℃).

2.4. Optical characterization

To elucidate the optical properties of the as-grown and annealed samples on SLG, both transmission and diffuse reflection spectra (normalized using same illumination area of dia~6 mm for all samples) were recorded. In the case of samples deposited on Cu foil, only the reflection spectra were taken. The diffuse reflection spectra of samples grown by sonication step less SILAR process at different temperatures of IPA dispersant are shown in Figure 4.

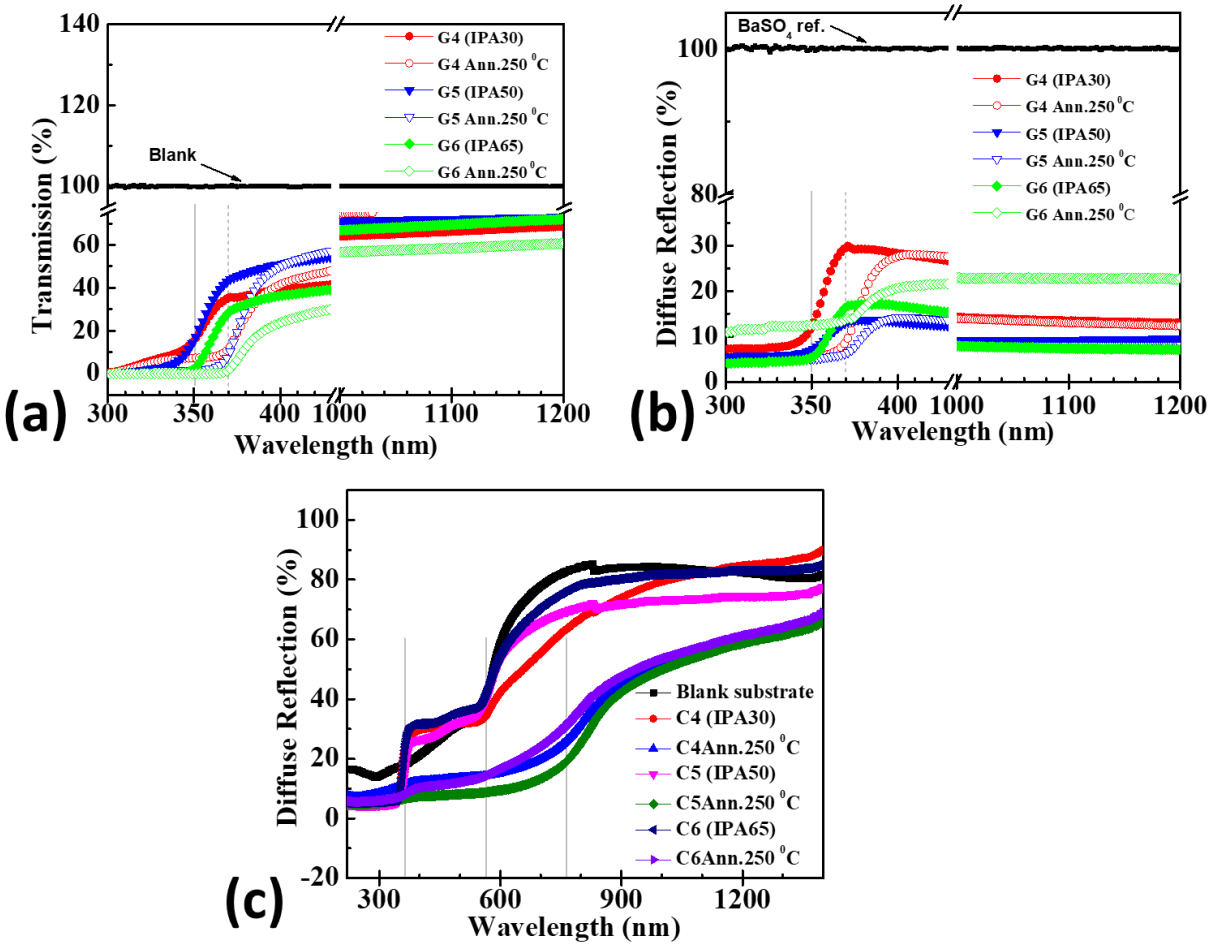

Figure 4. Normalized transmission (a) and diffuse reflection (b) spectra of the samples deposited on SLG substrate, and Normalized diffuse reflection spectra of the samples deposited on Cu foil (c). Both as-

deposited and annealed samples have been included in the same graph for comparison. The vertical lines are indicating the approximate absorption edge of ZnO, Cu_2O and CuO.

From Figure 4a, it is clearly seen that the samples grown on SLG shows roughly 35 - 65% transparency in the visible region. Upon post-annealing, the transparency of the films is seen to improve except for G6 Ann. 250 ^{0}C. The absorption edge is also seen to be shifted from the lower wavelength ($\lambda \approx 350$ nm, marked by solid line) to higher wavelength ($\lambda \approx 380$ nm,marked by dotted line) region (Figure 4a and Figure 4b) and such red shift of the absorption edges can be attributed to the crystalline improvement of the ZnO thin films.[36] From Figure 4b, samples grown with IPA dispersant at higher temperatures (50 and 65℃) exhibit red-shifted absorption edges which further confirms the better crystallinity and corroborates the XRD data. In contrast, for the samples grown on Cu foil (Figure 4c), sharp absorption edges near $\lambda \approx$380, 580 and 780 nm can clearly be seen (see fade vertical lines) which could be attributed to ZnO, Cu_2O and CuO phase respectively.[47,57,69] The presence of mixed (Cu_2O+CuO) phases formed on Cu foil were also confirmed from the XRD and Raman spectra shown in Figure 1b and Figure 2b.

The film thickness of the SILAR grown samples was estimated using simple gravimetric methods[47] and found to vary with number of dipping cycles, nature of the substrate surface, and other processing parameters which are listed in Table 3 in section 4.2. To avoid thickness variation related effects as well as substrate related issues, the optical bandgap was estimated from the Tauc plot generated by using the reflection data and the Kubelka-Munk function ($F(R_\infty)$[36] represented by equation:

$$(h\upsilon F(R_\infty))^n = A(h\upsilon - E_g) \quad (2)$$

Where, E_g= Bandgap energy, R_∞= Diffuse reflection, h= Planck's constant, and υ = Frequency of the incident light. ZnO is a direct bandgap material (n=2) which showed direct forbidden transition at wavelength $\lambda \approx$380 nm. Therefore, putting n = 2 in equation (2), the E_g value can be obtained by fitting a straight line to

the plot of $(h\upsilon F(R_\infty))^2$ *vs* $h\upsilon$ curve where the quantity $(h\upsilon F(R_\infty))^2$ is extrapolated to zero.[36,47] The bandgap plots are shown in Figure 5 and E_g values together with XRD and Raman data are summarized in Table 2.

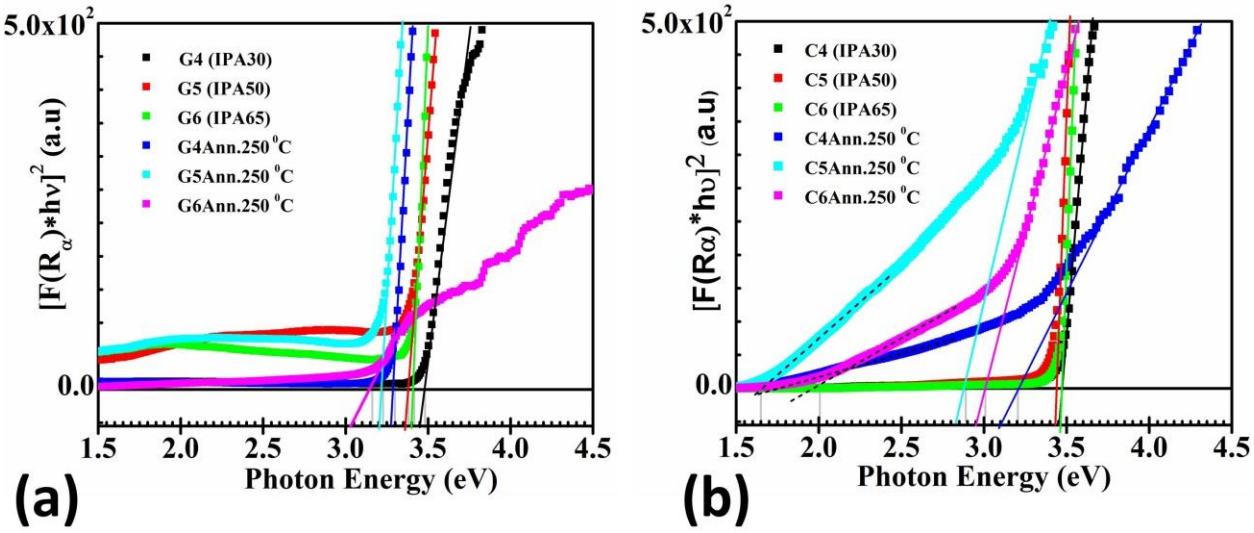

Figure 5. Tauc plots of the sonication steps less SILAR samples grown on **(a)** SLG **(b)** Cu foil using diffuse reflection data. The E_g values are calculated by extrapolating the quantity $(h\upsilon F(R_\infty))^2 = 0$

Table 2. Optical bandgap energy and phase identification evidenced from XRD and Raman spectra for as-deposited and annealed samples deposited at different temperature using IPA

Glass Samples	Band gap, Eg(eV) ± 0.01	Cu foil samples	Bandgap, Eg(eV) ± 0.01	Phase composition (XRD and Raman)
G4(IPA30)	3.48	C4(IPA30)	3.47	ZnO
G5(IPA50)	3.37	C5(IPA50)	3.43	ZnO
G6(IPA65)	3.40	C6(IPA65)	3.45	ZnO
G4 Ann. 250 ℃	3.28	C4 Ann. 250 ℃	1.65 &3.21	Cu_xO/ZnO
G5 Ann. 250 ℃	3.21	C5 Ann. 250 ℃	1.65 &2.98	Cu_xO/ZnO
G6 Ann. 250 ℃	3.15	C6 Ann. 250 ℃	2.00 &3.00	Cu_xO/ZnO

*Crystallite sizes of the samples grown on SLG substrate are shown in Table 1

From Table 2, it is clear that the $E_g$values are in the range of 3.37-3.47 eV for as-deposited samples and 2.98-3.28 eV for post-annealed samples which could be attributed to the ZnO. However, in case of Cu foil samples, post-annealing treatment exhibited additional E_g values in the range of 1.65 – 2.00 eV(see dotted line in Figure 5b) which could be attributed to the Cu_xO phase.[57] Notice that samples deposited on SLG exhibited a reduction in bandgap with increasing IPA temperatures due to improve crystallinity of the ZnO and consistent with the trend of crystallite sizes given in Table 1. Moreover, post-annealing treatment induced a significant reduction of E_g from ~3.4 eV to ~3.2 eV is presumably due to the improvement of crystallinity[5] with diminished micro-strain (see Table 1). These observations imply that post-annealing treatment at 250 ℃ impacted the films' optical properties largely compared to IPA temperatures. It is worth noting that samples grown on Cu-foil indicating the possibility of Cu_xO/ZnO junction formation by post-annealing (see Table 2). As a proof-of-concept, a preliminary heterojunction with Cu/Cu_xO/ZnO/Au structure was formed by a Cu-contact with Cu_xO layer (a part of thin films from the cell was scratched off) and a spring-loaded gold (Au) coated pin-contact with ZnO layer (See top-left inset in Figure 6a). The I-V characteristic curve of this cell under dark and white LED illumination confirmed the photo-response of Cu_xO/ZnO junction, which can be more conspicuously seen in the zoomed area of I-V curve near zero bias voltage (bottom-right inset in Figure 6a). Though a downward shift of the LED illuminated I-V curve is expected for Cu_xO/ZnO based solar, however, a similar but smaller downward shift of the dark I-V curve may suggest a non-ideal probing contact of the present cell structure. Even though a metallic aluminum (Al) would be a good ohmic contact for ZnO layer, spring-loaded Au coated pin-contact formed reasonably good ohmic contact as can be seen from Figure 6b (the inset shows the photograph of Au/ZnO/Au probing arrangement). The diffuse reflection of the same cell at two different areas confirmed the formation Cu_xO layer (see Figure 4**c**) in the Cu_xO/ZnO based heterojunction (cf. Figure 6c and cf. Figure 4c). However, further experimental investigations are in progress to optimize the cell structure as well as to assess photovoltaic performance of SILAR grown Cu_xO/ZnO junctions.

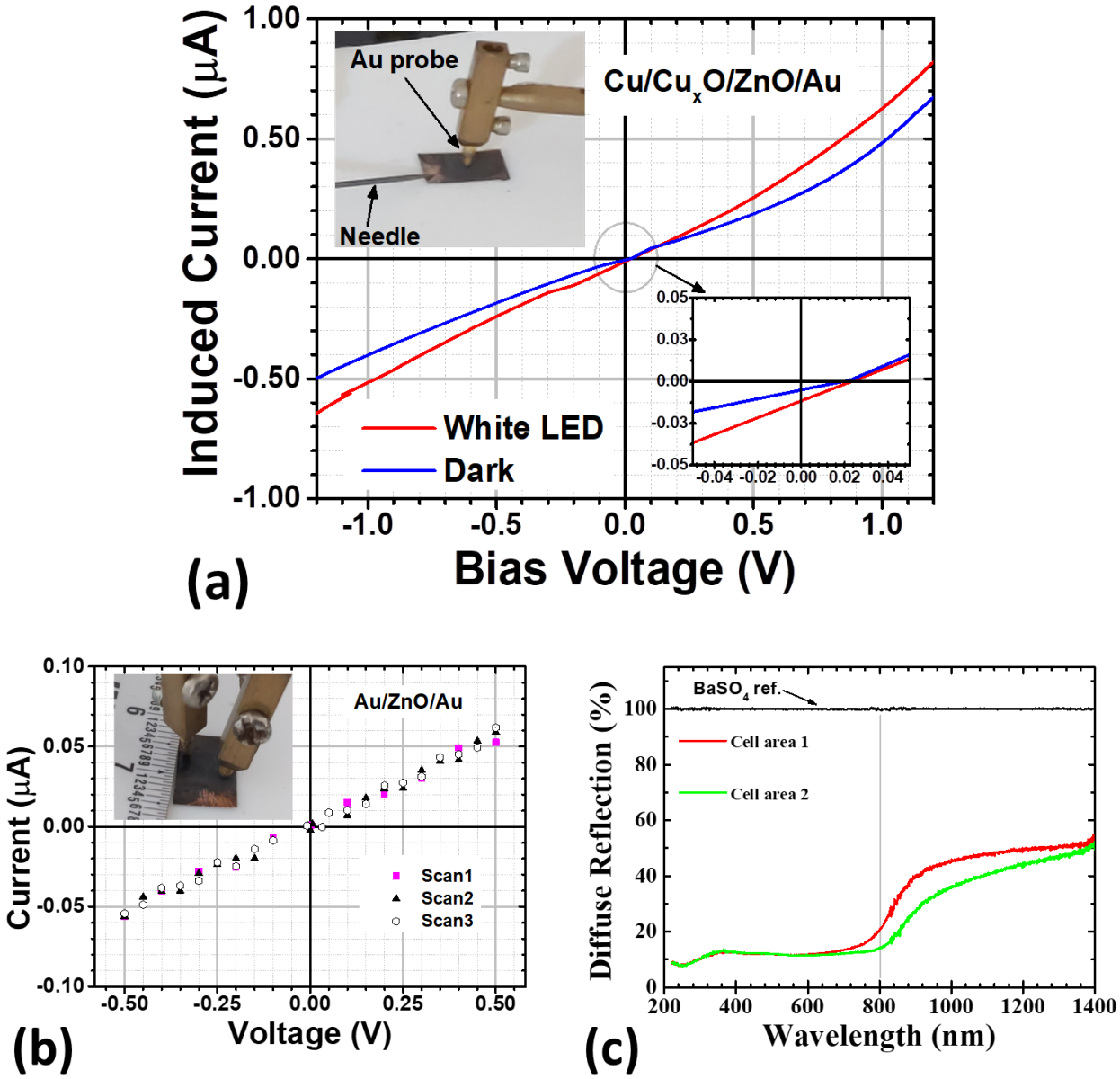

Figure 6. A typical SILAR Grown ZnO layer (IPA50) grown on Cu foil followed by the air-annealing at 250 ^{0}C for 1 h for the formation of Cu$_x$O/ZnO junction: **(a)** I-V characteristic curve of a typical Cu/Cu$_x$O/ZnO/Au structure under dark and white LED illumination (top-left inset shows the photograph of cell contact, bottom-right inset shows the zoomed area of the I-V curve marked by fade circle; **(b)** I-V characteristic curve of the ZnO layer with Au contact showing ohmic behavior (inset shows the

photograph of the ohmic contact with Au coated probes), **(c)** Diffuse reflection measured at two different area of the same cell showing the formation of Cu_xO layer.

3. CONCLUSIONS

In this work, ZnO thin films have been synthesized on both SLG and Cu foil and the effect of substrate, sonication process, and post-annealing on the properties of the deposited films were systematically investigated. XRD analysis revealed the growth of highly crystalline *c*-axis oriented ZnO thin films on SLG with (002) preferred orientation and (101) preferential growth on Cu foil. XRD and Raman spectroscopy confirmed that post-annealing treatment of Cu foil samples produced Cu_xO/ZnO heterojunctions irrespective to the SILAR processing parameters studied. Samples deposited by sonication less SILAR process exhibited compact and uniformly distributed grain surface morphologies in the presence of IPA at 50 and 65 ℃ evident from SEM micrographs. The estimated optical bandgap for as-deposited samples is in the range of 3.47-3.37 eV for as-deposited samples and found to be reduced significantly after post-annealing treatment at 250 ^{0}C due to the crystallinity improvement of ZnO thin films. The sample grown at 50 ℃ revealed the best quality film grown in this work with a bandgap value of 3.37 eV. This study proposed that for highly *c*-axis oriented ZnO thin films, it may be better to deposit the films on SLG by sonication less SILAR process using IPA as a dispersing agent. We hope that this study will open up a new approach for growing ZnO thin film with less processing steps as well as solution processable Cu-oxide/ZnO heterojunctions for diverse applications.

4. MATERIALS AND METHODS

4.1. Materials

In this work, zinc chloride ($ZnCl_2$, purity~ 98%, Scharlau), isopropyl alcohol ($(CH_3)_2CHOH$, purity ~99.70%, Active Fine Chemicals), and concentrated ammonia (NH_4OH, ~28% solution, Merck Millipore) were used. All the reagents were of analytical grade and used without further purification. Both non-conducting SLG (40×25×1 mm^3) and conducting thin Cu foil (40×20×0.2 mm^3) were used to deposit ZnO thin films.

4.2. Synthesis of ZnO Thin Films

ZnO thin films were deposited simultaneously both on SLG and Cu foil substrates by using a similar SILAR method described elsewhere.[47] Briefly, the SLG were cleaned with detergent followed by successive cleaning steps in an ultrasonic bath using DI water, toluene, acetone, isopropyl alcohol, and again DI water, each step for 15 min. On the other hand, Cu foils were treated with cotton wood soaked in 10 M HNO_3 solution and finally dried in air. Prior to the film deposition, zinc complex ($[Zn(NH_3)_4]^{2+}$) precursor solution was prepared by mixing 0.1 M $ZnCl_2$ and concentrated (~28 %) ammonia solution (NH_4OH). Additional NH_4OH was added dropwise into it up to the pH 10.[52,53] Subsequently, both SLG and Cu foil(tied back to back)[47] were immersed together into the precursor zinc-complex solution and then dipped into unheated deionized water each for 20 s which results in the formation of $Zn(OH)_2$ precipitate on the substrate. Then, counter ion (Cl^-) and loosely adhered $Zn(OH)_2$ species were removed from the substrate surface by immersing it into ultrasonic-assisted DI water (through **III'** and **V** steps shown in Figure 7) or ultrasonication-less DI water (through **III** and **IV** steps shown in Figure 7) for 30 s. In between the DI water steps, the precursor coated substrates were treated with IPA for 20 s to form ZnO (either through **IV'** or **IV** steps shown in Figure 7) layer atop the substrate surface.

The overall reactions involved in the ZnO film deposition are given below[5]:

$$[Zn(NH_3)_4]^{2+} + 4H_2O \longrightarrow Zn^{2+} + 4NH_4^+ + 4OH^-$$

$$Zn^{2+} + 2OH^- \longrightarrow Zn(OH)_2(s)$$

$$Zn(OH)_2(s) \longrightarrow ZnO(s) + H_2O$$

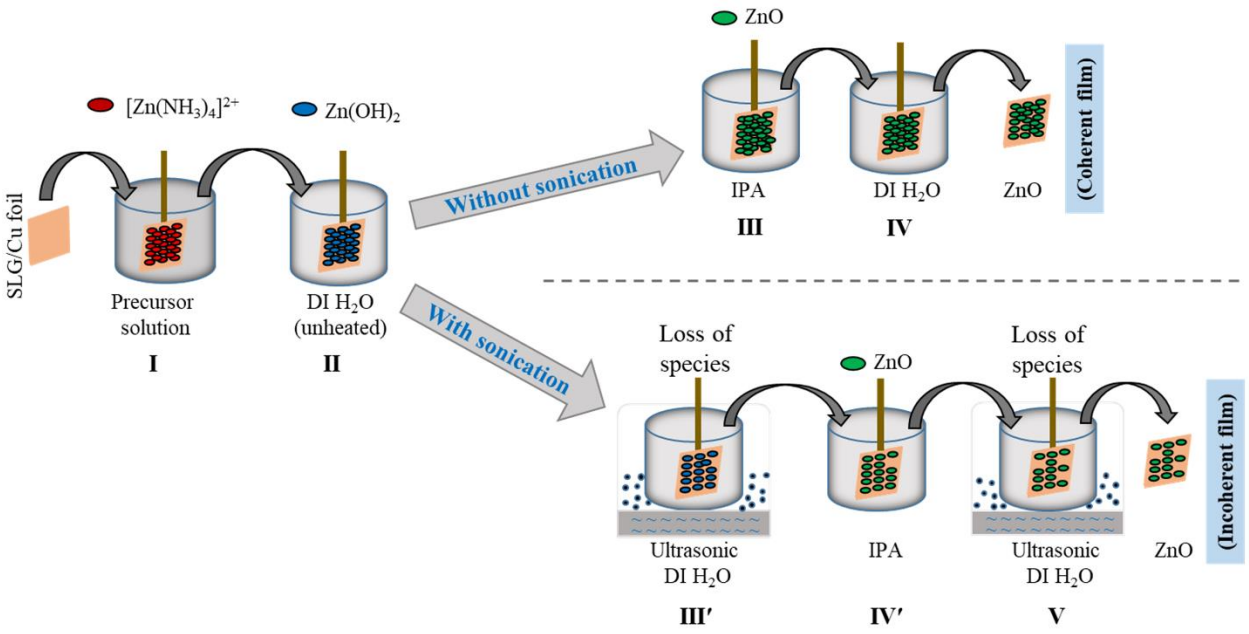

Figure 7. A schematic diagram showing the SILAR deposition of ZnO thin film simultaneously on SLG and Cu foil substrates using IPA dispersant. The optimized deposition process (scheme above the dotted line) facilitates to produce coherent thin films by eliminating the ultrasonication steps (**III'** and **V**).

Here, IPA acted as a dispersing agent which reduced the ZnO agglomeration and enhanced the decomposition capability of $Zn(OH)_2$ to ZnO when the temperature was increased from room temperature (~30℃) to 65 ℃. The above steps were repeated up to 20 times for preparing the sample with IPA at 30, 50, and 65℃ and labeled the as-deposited samples as IPA30, IPA50, and IPA65 respectively. The most important deposition parameters and processing conditions (including the estimated thickness of the samples) are summarized in Table 3. After deposition, the samples were thoroughly rinsed by DI water, and then dried under laboratory atmosphere and safely stored into the sample boxes for various characterizations. Some of the samples were cut into equal pieces for subsequent characterizations as well as 1 h air-annealing at 250 ℃; while one piece of each batch was kept as as-deposited sample for reference. The surface morphology analyses of the deposited films by SEM revealed that sonication-less SILAR process produced coherent films compared to sonication-assisted SILAR process. This can be understood

as follows: loosely adsorbed $[Zn(NH_3)_4]^{2+}$ ions as well as $Zn(OH)_2$ species on substrate surface were more prone to wash away during the immersion in **III'** and **V** steps owing to ultrasonication compared to the scheme involved in **III** and **IV** steps. Therefore, overall, less amount of precursor species (see Figure 7) is available to convert into ZnO solid atop the substrate surface, thereby sonication-assisted SILAR process produced incoherent films.

Table 3. Sampling details for the deposition of ZnO thin films with IPA at different temperatures. The thickness and number of dipping cycle associated with the deposited films are shown in the parentheses.

Deposition temperature (^{0}C)	Glass substrate thickness (nm)		Copper foil substrate thickness (nm)	
	Sonication	*Without sonication*	*Sonication*	*Without sonication*
30 (20 cycle)	G1(136±34)	G4(380±19)	C1(364±11)	C4(438±10)
50 (20 cycle)	G2(660±12)	G5(864±22)	C2(283±10)	C5(848±11)
50 (30 cycle)	-	3330±87	-	2660±64
50 (40 cycle)	-	8780±219	-	7870±228
65 (20 cycle)	G3(470±10)	G6(960±18)	C3(318±11)	C6(955±95)

4.3. Characterization techniques

The structural properties and phase of the deposited thin films were investigated by XRD (Philips PANalytical X'Pert MRD) with a CuKα (λ = 0.15406 nm) radiation source in θ-2θ coupled mode and Raman spectroscopy (Horiba HR800) with 488 nm laser excitation (Power ≤ 5 mW). The Raman spectrometer was calibrated by using a standard silicon sample with respect to the 520 cm^{-1} line prior to the recording of the spectra of deposited samples. Surface morphologies of the samples were imaged by a scanning electron microscope (SEM) (Philips XL30 EEG SEM). The optical properties were examined by using a double-beam

UV-Visible-NIR spectrophotometer (Shimadzu UV 2600 ISR plus) in the range of 220-1200 nm. Both diffuse reflection and transmission spectra were taken to eliminate substrate contributions[36] form the thin film where necessary. Dark and LED (white) illuminated I-V curve of the SILAR grown Cu_xO/ZnO junctions including ohmic contact nature on the ZnO layer were recorded by a Keithley 2450 source measure unit (SMU) coupled with a homemade multiprobe workstation (IPD, BCSIR).

AUTHOR INFORMATION

Corresponding Author

Syed Farid Uddin Farhad - *Energy Conversion and Storage Research Section, Industrial Physics Division, BCSIR Labs, Dhaka 1205, Bangladesh Council of Scientific and Industrial Research (BCSIR), Bangladesh;* ***Email:*** sf1878@my.bristol.ac.uk; *Phone: +8801881755767*

ORCID iD

Syed Farid Uddin Farhad: https://orcid.org/0000-0002-0618-8679

Authors

Bijoy Chandra Ghos - *Department of Chemistry, Comilla University, Cumilla-3506, Bangladesh.*

Md Abdul Majed Patwary - *Department of Chemistry, Comilla University, Cumilla-3506, Bangladesh.*

Shanta Majumder - *Department of Chemistry, Comilla University, Cumilla-3506, Bangladesh.*

Md. Alauddin Hossain - *Department of Chemistry, Comilla University, Cumilla-3506, Bangladesh.*

Nazmul Islam Tanvir - *Energy Conversion and Storage Research Section, Industrial Physics Division, BCSIR Labs, Dhaka 1205, Bangladesh Council of Scientific and Industrial Research (BCSIR), Bangladesh.*

Mohammad Atiqur Rahman - *Department of Chemistry, Comilla University, Cumilla-3506, Bangladesh.*

Tooru Tanaka - *Department of Electrical and Electronic Engineering, Saga University, Honjo, Saga 840-8502, Japan.*

Qixin Guo - *Department of Electrical and Electronic Engineering, Saga University, Honjo, Saga 840-8502, Japan.*

AUTHOR CONTRIBUTION

B. C. Ghos performed the sample synthesis, data analysis and wrote the preliminary manuscript. S. F. U. Farhad conceived the project idea and designed experimental works, conceptualization, edited the

manuscript, and led the overall research works. M. A. M. Patwary and N. I. Tanvir supported with the experimental methodology and characterization setups. S.F.U. Farhad, S. Majumder, M. A. Hossain, and M.A. Rahman have contributed to the formal data analyses and scientific discussion of the results. Q. Guo supported with the Raman setup while T. Tanaka with the XRD and SEM setups as well as discussions. All authors contributed to the writing, reviewing and editing of the final manuscript.

ACKNOWLEDGMENTS

S.F.U. Farhad and N.I. Tanvir gratefully acknowledge the experimental support of the Energy Conversion and Storage Research (ECSR) Section, Industrial Physics Division (IPD), BCSIR Laboratories, Dhaka 1205, Bangladesh Council of Scientific and Industrial Research (BCSIR) under the scope of R&D project#100-FY2017-2020 and S.F.U. Farhad also acknowledges the support of TWAS grant#20-143 RG/PHYS/AS_I for ECSR, IPD. M.A.M. Patwary, T. Tanaka, and Q. Guo acknowledge the characterization support of Department of Electrical and Electronic Engineering, Saga University, Japan.

DATA AVAILABILITY

All data provided in this manuscript and supporting materials are self-explanatory. There is no extra-data information which has been used in support of the arguments/result-explanations presented in the manuscript and supporting materials. However, the raw data used for generating the graph(s) in the manuscript and supporting materials will be made available on request. Notice, some explicitly related data could not be disclosed as they will be used for future scientific communication(s).

Conflicts of Interest: The authors declare no competing financial interest.

TOC graphic

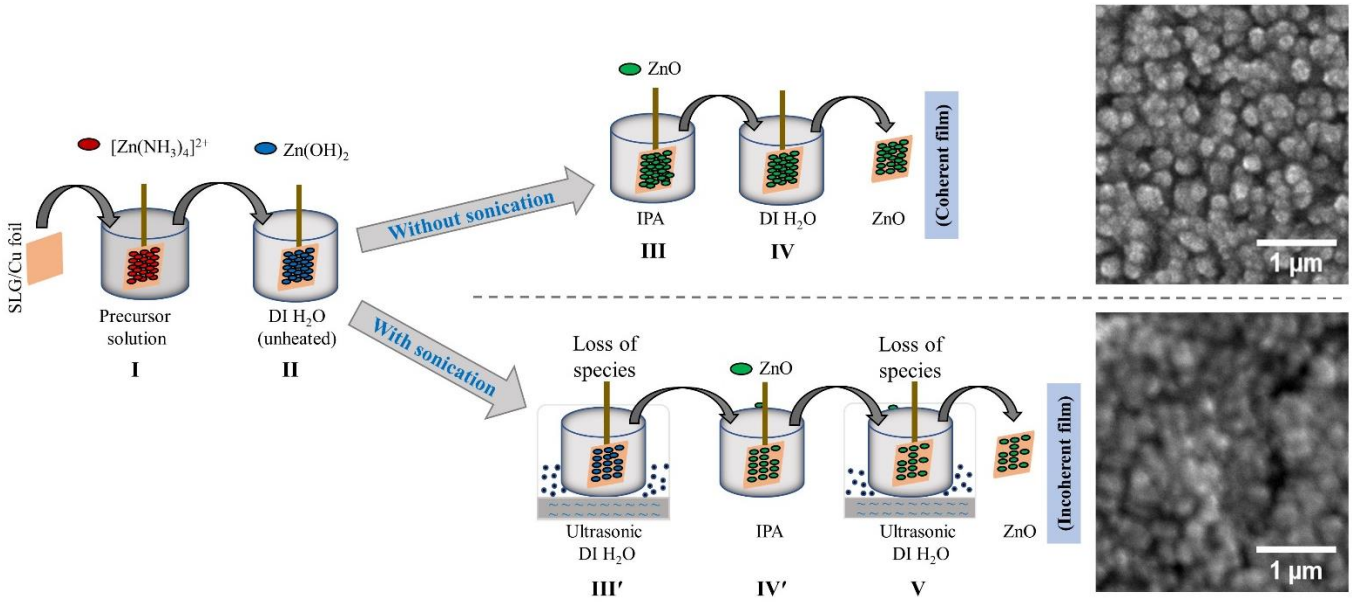

REFERENCES

(1) Akhta, M. S.; Riaz, S.; Noor, R.; Naseem, S. Optical and structural properties of ZnO thin films for solar cell applications. *Adv Sci Lett*. **2013**, *19*, 834-838. https://doi.org/10.1166/asl.2013.4822

(2) Muchuweni, E, Sathiaraj, T. S.; Nyakotyo, H. Physical properties of gallium and aluminium co-doped zinc oxide thin films deposited at different radio frequency magnetron sputtering power. *Ceram Int*. **2016**, *42*, 17706-17710. https://doi.org/10.1016/j.ceramint.2016.08.091

(3) Lu, H. C.; Jou, J. C.; Chu, C. L.; Influence of RF magnetron sputtering conditions on the properties of transparent conductive gallium-doped magnesium zinc oxide thin films. *Surf Coatings Technol*. **2013**, *231*, 539-542. https://doi.org/10.1016/j.surfcoat.2012.10.029

(4) Ashfold, M. N. R.; Doherty, R. P.; Ndifor-Angwafor, N. G.; Riley, D. J.; Sun, Y. The kinetics of the hydrothermal growth of ZnO nanostructures. *Thin Solid Films*. **2007**, *515*, 8679-8683. https://doi.org/10.1016/j.tsf.2007.03.122

(5) Shei, S. C.; Lee, P. Y. Influence of rinsing temperature on properties of ZnO thin films prepared by SILAR method with propylene glycol. *J Alloys Compd*. **2013**, *546*, 165-170. https://doi.org/10.1016/j.jallcom.2012.07.149

(6) Joshi, K.; Rawat, M.; Gautam, S. K.; Singh, R. G.; Ramola, R. C.; Singh, F. Band gap widening and narrowing in Cu-doped ZnO thin films. *J Alloys Compd*. **2016**, *680*, 252-258. https://doi.org/10.1016/j.jallcom.2016.04.093

(7) Rong, P.; Ren, S.; Yu, Q. Fabrications and Applications of ZnO Nanomaterials in Flexible Functional Devices-A Review. *Crit Rev Anal Chem*. **2019**, *49*, 336-349. https://doi.org/10.1080/10408347.2018.1531691

(8) Aoun, Y.; Benhaoua, B.; Benramache, S.; Gasmi, B. Effect of deposition rate on the structural, optical and electrical properties of Zinc oxide (ZnO) thin films prepared by spray pyrolysis technique. *Optik (Stuttg)*. **2015**, *126*, 2481-2484. https://doi.org/10.1016/j.ijleo.2015.06.025

(9) Gil, B.; Kavokin, A. V. Giant exciton-light coupling in ZnO quantum dots. *Appl Phys Lett*. **2002**, *81*, 748-750. https://doi.org/10.1063/1.1494864

(10) Bretagnon, T.; Lefebvre, P.; Valvin, P.; Gil, B.; Morhain, C.; Tang, X. Time resolved photoluminescence study of ZnO/(Zn,Mg)O quantum wells. *J Cryst Growth*. **2006**, *287*, 12-15. https://doi.org/10.1016/j.jcrysgro.2005.10.034

(11) Xiong, C.; Yao, R. H.; Wan, W. J.; Xu, J. X. Fabrication and electrical characterization of ZnO rod arrays/CuSCN heterojunctions. *Optik (Stuttg)*. **2014**, *125*, 785-788. https://doi.org/10.1016/j.ijleo.2013.07.080

(12) Hassan, M. A. M.; Saleh, A. F.; Mezher, S. J. Energy band diagram of In: ZnO/p-Si structures deposited using chemical spray pyrolysis technique. *Appl Nanosci*. **2014**, *4*, 695-701. https://doi.org/10.1007/s13204-013-0246-5

(13) Manoharan, C.; Pavithra, G.; Bououdina, M.; Dhanapandian, S.; Dhamodharan, P. Characterization and study of antibacterial activity of spray pyrolysed ZnO:Al thin films. *Appl Nanosci*. **2016**, *6*, 815-825. https://doi.org/10.1007/s13204-015-0493-8

(14) Balaji, G.; Sivakami, R.; Sridharan, M.; Jeyadheepan, K. Preparation and Characterization of

Refractory ZnO Buffer Layers for Thin Film Solar Cell Applications. *Mater Today Proc*. **2016**, *3*, 1730-1736. https://doi.org/10.1016/j.matpr.2016.04.067

(15) Aoun, Y.; Benhaoua, B.; Benramache, S.; Gasmi, B. Effect of annealing temperature on structural, optical and electrical properties of zinc oxide (ZnO) thin films deposited by spray pyrolysis technique. *Optik (Stuttg)*. **2015**, *126*, 5407-5411. https://doi.org/10.1016/j.ijleo.2015.08.267

(16) Islam, M. R.; Podder, J.; Farhad, S. F. U.; Saha, D. K. Effect of annealing on the structural and optical properties of nano fiber ZnO films deposited by spray pyrolysis. *Sensors and Transducers*. **2011**, *134*, 170-176.

(17) Kowsar, A.; Rahaman, M.; Islam, M. S.; Imam, A. Y.; Debnath, S. C.; Sultana, M.; Hoque, M. A.; Sharmin, A.; Mahmood, Z. H.; Farhad, S. F. U. Progress in Major Thin-Film Solar Cells: Growth Technologies, Layer Materials and Efficiencies. *Int Journal of Renewable Energy Research.* **2019**, *9*

(18) Dhanakodi, K.; Thirunavukkarasu, P.; Mariappan, R.; Rajamanickam, A. T. Effect of substrate temperature on the nebulizer sprayed zinc oxide thin films. *Optik (Stuttg)*. **2016,** *127*, 2516-2520. https://doi.org/10.1016/j.ijleo.2015.10.143

(19) Kenanakis, G.; Katsarakis, N.; Koudoumas, E. Influence of precursor type, deposition time and doping concentration on the morphological, electrical and optical properties of ZnO and ZnO:Al thin films grown by ultrasonic spray pyrolysis. *Thin Solid Films*. **2014**, *555*, 62-67. https://doi.org/10.1016/j.tsf.2013.10.015

(20) Zhang, Z.; Liao, Q.; Yu, Y.; Wang, X.; Zhang, Y. Enhanced photoresponse of ZnO nanorods-based self-powered photodetector by piezotronic interface engineering. *Nano Energy*. **2014**, *9*, 237-244. https://doi.org/10.1016/j.nanoen.2014.07.019

(21) Roy, S.; Banerjee, N.; Sarkar, C. K.; Bhattacharyya, P. Development of an ethanol sensor based on CBD grown ZnO nanorods. *Solid. State. Electron.* **2013,** *87*, 43–50. https://doi.org/10.1016/j.sse.2013.05.003.

(22) Singh, O.; Kohli, N.; Singh, R. C. Precursor controlled morphology of zinc oxide and its sensing behaviour. *Sensors Actuators B Chem.* **2013**, *178*, 149–154. https://doi.org/10.1016/j.snb.2012.12.053.

(23) Schmidt-Mende, L.; MacManus-Driscoll, J. L. ZnO - nanostructures, defects, and devices. *Mater. Today.* **2007**, *10,* 40–48. https://doi.org/10.1016/S1369-7021(07)70078-0.

(24) Kadota, M. Surface acoustic wave characteristics of a ZnO/quartz substrate structure having a large electromechanical coupling factor and a small temperature coefficient. *Japanese J. Appl. Physics.* **1997**, *36*, 3076–3080. https://doi.org/10.1143/jjap.36.3076.

(25) Ennaceri, H.; Erfurt, D.; Wang, L.; Köhler, T.; Taleb, A.; Khaldoun, A.; El Kenz, A.; Benyoussef, A.; Ennaoui, A. Deposition of multifunctional TiO_2 and ZnO top-protective coatings for CSP application. *Surf. Coatings Technol.* **2016,** *298*, 103–113. https://doi.org/10.1016/j.surfcoat.2016.04.048.

(26) Lin, Z.; Song, J. Piezoelectric Nanogenerators Based on Zinc Oxide Nanowire Arrays. *Science.* **2006,** *312*, 242–246. https://doi.org/10.1126/science.1124005.

(27) Lee, P. Y.; Chang, S. P.; Chang, J. F.; Hsu, E. N.; Chang, S. J. Highly Transparent Nanostructured Zinc Oxide Photodetector Prepared by Successive Ionic Layer Adsorption and Reaction. *Int. J. Electrochem. Sci.* **2013,** *8*, 6425–6432.

(28) Xiangdong, G.; Xiaomin, L.; Weidong, Y. Preparation and Characterization of Highly Oriented ZnO Film by Ultrasonic Assisted SILAR Method. *J. Wuhan Univ. Technol. - Mater. Sci.* **2005,** *20*, 23-26. https://doi.org/10.1007/BF02835019.

(29) Ajuba, A. E.; Ezugwu, S. C.; Ezekoye, B. A.; Ezema, F. I.; Asogwa, P. U. Influence of pH on the structural, optical and solid state properties of chemical bath deposited ZnO thin films. *Journal of Optoelectronics and Biomedical Materials*. **2010,** *2 (2)*, 73–78.

(30) Farhad, S. F. U. The effect of substrate temperature and oxygen partial pressure on the properties of nanocrystalline copper oxide thin films grown by pulsed laser deposition. *Data in Brief*. **2020** (accepted). http://dx.doi.org/10.17632/rmzrnz2nd7.3.

(31) Alfaro Cruz, M. R.; Ceballos-Sanchez, O.; Luévano-Hipólito, E.; Torres-Martínez, L. M. ZnO thin films deposited by RF magnetron sputtering: Effects of the annealing and atmosphere conditions on the photocatalytic hydrogen production. *Int. J. Hydrogen Energy*. **2018,** *43*, 10301–10310. https://doi.org/10.1016/j.ijhydene.2018.04.054.

(32) Ye, J.; Gu, S.; Zhu, S.; Chen, T.; Hu, L.; Qin, F.; Zhang, R.; Shi, Y.; Zheng, Y. The growth and annealing of single crystalline ZnO films by low-pressure MOCVD. *J. Cryst. Growth.* **2002,** *243*, 151–156. https://doi.org/10.1016/S0022-0248(02)01474-4.

(33) Islam, M. R.; Rahman, M.; Farhad, S. F. U.; Podder, J. Structural, optical and photocatalysis properties of sol–gel deposited Al-doped ZnO thin films. *Surfaces and Interfaces*. **2019,** *16*, 120–126. https://doi.org/10.1016/j.surfin.2019.05.007.

(34) Baruah, S.; Dutta, J. Effect of seeded substrates on hydrothermally grown ZnO nanorods. *J. Sol-Gel Sci. Technol.* **2009**, *50*, 456–464. https://doi.org/10.1007/s10971-009-1917-2.

(35) Kato, H.; Sano, M.; Miyamoto, K.; Yao, T. High-quality ZnO epilayers grown on Zn-face ZnO substrates by plasma-assisted molecular beam epitaxy. *J. Cryst. Growth.* **2004**, *265*, 375–38. https://doi.org/10.1016/j.jcrysgro.2004.02.021.

(36) Farhad, S. F. U.; Tanvir, N. I.; Bashar, M. S.; Hossain, M. S.; Sultana, M.; Khatun, N. Facile synthesis of oriented zinc oxide seed layer for the hydrothermal growth of zinc oxide nanorods. *Bangladesh J. Sci. Ind.* **2018,** *53*, 233–244. https://doi.org/10.3329/bjsir.v53i4.39186.

(37) Pelicano, C. M.; Yanagi, H. pH-controlled surface engineering of nanostructured ZnO films generated via a sustainable low-temperature H_2O oxidation process. *Appl Surf Sci*. **2019**, *467-468*, 932-939. https://doi.org/10.1016/j.apsusc.2018.10.254

(38) Pelicano, C. M.; Yanagi, H. Effect of rubrene:P3HT bilayer on photovoltaic performance of perovskite solar cells with electrodeposited ZnO nanorods. *J Energy Chem*. **2018,** *27*, 455-462. https://doi.org/10.1016/j.jechem.2017.11.018

(39) Felizco, J. C; Uenuma, M.; Juntunen, T.; Etula, J.; Tossi, C.; Ishikawa, Y.; Tittonen, I. J.; Uraoka, Y. Enhanced thermoelectric transport and stability in atomic layer deposited-HfO_2/ZnO and TiO_2/ZnO-sandwiched multilayer thin films. *ACS Appl Mater Interfaces*. **2020**, *12*, 49210-49218. https://doi.org/10.1021/acsami.0c11439

(40) Frahad, S. F. U.; Tanvir, N. I.; Bashar, M. S.; Sultana, M. Synthesis and characterization of c-axis oriented Zinc Oxide thin films and its use for the subsequent hydrothermal growth of Zinc Oxide nanorods. *MRS Adv.* **2019**, *4*, 921–928. https://doi.org./10.1557/adv.2019.65.

(41) Asim, N.; Ahmadi, S.; Alghoul, M. A.; Hammadi, F. Y.; Saeedfar, K.; Sopian, K. Research and development aspects on chemical preparation techniques of photoanodes for dye sensitized solar cells. *Int J Photoenergy*. **2014.** https://doi.org./10.1155/2014/518156

(42) Ojo, A. A.; Dharmadasa, I. M. Electroplating of semiconductor materials for applications in large area electronics: A review. *Coatings*. **2018**, *8*. https://doi.org./10.3390/coatings8080262

(43) Su, Z.; Sun, K.; Han, Z.; Liu, F.; Lai, Y.; Li, J.; Liu, Y. Fabrication of ternary Cu-Sn-S sulfides by a modified successive ionic layer adsorption and reaction (SILAR) method. *J. Mater. Chem.* **2012,** *22*, 16346–16352. https://doi.org/10.1039/c2jm31669b.

(44) Dhaygude, H. D.; Shinde, S. K.; Velhal, N. B.; Lohar, G. M.; Fulari, V. J. Synthesis and characterization of ZnO thin film by low cost modified SILAR technique. *AIMS Mater. Sci.* **2016**, *3*, 349–356. https://doi.org/10.3934/matersci.2016.2.349.

(45) Raidou, A.; Benmalek, F.; Sall, T.; Aggour, M.; Qachaou, A.; Laanab, L.; Fahoume, M. Characterization of ZnO Thin Films Grown by SILAR Method. *OALib.* **2014**, *01*, 1–9. https://doi.org/10.4236/oalib.1100588.

(46) Offiah, S. U.; Agbo, S. N.; Sutta, P.; Maaza, M.; Ugwuoke, P. E.; Osuji, R. U.; Ezema, F. I. Study of the extrinsic properties of ZnO:Al grown by SILAR technique. *J. Solid State Electrochem.* **2017**, *21*, 2621–2628. https://doi.org/10.1007/s10008-017-3514-6.

(47) Farhad, S.F.U.; Hossain, M. A.; Tanvir, N. I.; Akter, R.; Patwary, M. A. M.; Shahjahan, M.; Rahman, M. A. Structural, optical, electrical, and photoelectrochemical properties of cuprous oxide thin films grown by modified SILAR method. *Mater. Sci. Semicond. Process.* **2019,** *95*, 68–75. https://doi.org/10.1016/j.mssp.2019.02.014.

(48) Mageshwari, K.; Sathyamoorthy, R. Physical properties of nanocrystalline CuO thin films prepared by the SILAR method. *Mater. Sci. Semicond. Process.* **2013,** *16*, 337–343. https://doi.org/10.1016/j.mssp.2012.09.016.

(49) Patil, A. S.; Lohar, G. M; Fulari, V. J. Structural, morphological, optical and photoelectrochemical cell properties of copper oxide using modified SILAR method. *J. Mater. Sci. Mater. Electron.* **2016,** *27*, 9550–9557. https://doi.org/10.1007/s10854-016-5007-2.

(50) Beaini, S. S.; Kronawitter, C. X.; Carey, V. P.; Mao, S. S. ZnO deposition on metal substrates: Relating fabrication, morphology, and wettability. *J. Appl. Phys.* **2013,** *113*, 184905. https://doi.org/10.1063/1.4803553.

(51) Raidou, A.; Lharch, M.; Nouneh, K.; Aggour, M.; Qachaou, A.; Laanab, L.; Fahoume, M. Effect of substrate on ZnO thin films grown by SILAR method. *Int. Renew. Sustain. Energy Conf. IRSEC.* **2014**. 695–700. https://doi.org/10.1109/IRSEC.2014.7059829.

(52) Shei, S. C.; Lee, P. Y.; Chang, S. J. Effect of temperature on the deposition of ZnO thin films by successive ionic layer adsorption and reaction. *Appl. Surf. Sci.* **2012**, *258*, 8109–8116. https://doi.org/10.1016/j.apsusc.2012.05.004.

(53) Shei, S. C.; Chang, S. J.; Lee, P. Y. Rinsing Effects on Successive Ionic Layer Adsorption and Reaction Method for Deposition of ZnO Thin Films. *J. Electrochem. Soc.* **2011,** *158*, H208. https://doi.org/10.1149/1.3528306.

(54) Farhad, S. F. U.; Majumder, S.; Hossain, M. A.; Tanvir, N. I.; Akter, R.; Patwary, M. A. M. Effect of Solution pH and Post-annealing temperatures on the Optical Bandgap of the Copper Oxide Thin

Films Grown by modified SILAR Method. *MRS Adv.* **2019,** *4*, 937–944. https://doi.org/https://doi.org/10.1557/adv.2019.139.

(55) Chowdhury, R. I.; Hossen, M. A.; Mustafa, G.; Hussain, S.; Rahman, S. N.; Farhad, S. F. U.; Murata, K.; Tambo, T.; Islam, A. B. M. O. Characterization of chemically deposited cadmium sulfide thin films. *Int. J. Mod. Phys. B.* **2010**, *24*, 5901–5911. https://doi.org/10.1142/S0217979210055147.

(56) Rosenberg, Y.; Machavariani, V. S.; Voronel, A.; Garber, S.; Rubshtein, A.; Frenkel, A. I.; Stern, E. A. Strain energy density in the X-ray powder diffraction from mixed crystals and alloys. *J Phys Condens Matter*. **2000**, *12*, 8081-8088. https://doi.org/10.1088/0953-8984/12/37/307

(57) Farhad, S. F. U.; Webster, R. F.; Cherns, D. Electron microscopy and diffraction studies of pulsed laser deposited cuprous oxide thin films grown at low substrate temperatures. *Materialia.* **2018**, *3*, 230–238. https://doi.org/10.1016/j.mtla.2018.08.032.

(58) Singh, S.; Srinivasa, R. S.; Major, S. S. Effect of substrate temperature on the structure and optical properties of ZnO thin films deposited by reactive rf magnetron sputtering. *Thin Solid Films.* **2007**, *515*, 8718–8722. https://doi.org/10.1016/j.tsf.2007.03.168.

(59) Patwary, M. A. M.; Saito, K.; Guo, Q.; Tanaka, T. Influence of oxygen flow rate and substrate positions on properties of Cu-oxide thin films fabricated by radio frequency magnetron sputtering using pure Cu target. *Thin Solid Films.* **2019,** *675,* 59–65. https://doi.org/10.1016/j.tsf.2019.02.026.

(60) Koyano, M.; QuocBao, P.; ThanhBinh, L. T.; HongHa, L.; NgocLong, N.; Katayama, S. Photoluminescence and Raman spectra of ZnO thin films by charged liquid cluster beam technique. *Phys. Status Solidi Appl.* **2002**, *193*, 125–131. https://doi.org/10.1002/1521-396X(200209)193:1<125::AID-PSSA125>3.0.CO;2-X.

(61) Yahia, S. B.; Znaidi, L.; Kanaev, A.; Petitet, J. P. Raman study of oriented ZnO thin films deposited by sol-gel method. *Spectrochim. Acta - Part A Mol. Biomol. Spectrosc.* **2008**, *71*, 1234–1238. https://doi.org/10.1016/j.saa.2008.03.032.

(62) Farhad, S. F. U.; Cherns, D.; Smith, J. A.; Fox, N. A.; Fermín, D, J. Pulsed laser deposition of single phase n- and p-type Cu_2O thin films with low resistivity. *Mater. Des.* **2020**, *193*, 108848. https://doi.org/10.1016/j.matdes.2020.108848.

(63) Patwary, M. A. M.; Ho, C. Y.; Saito, K.; Guo, Q.; Yu, K. M.; Walukiewicz, W.; Tanaka, T. Effect of oxygen flow rate on properties of Cu_4O_3 thin films fabricated by radio frequency magnetron sputtering. *J. Appl. Phys.* **2020**, *127*, 085302. https://doi.org/10.1063/1.5144205.

(64) Pandey, P.; Parra, M. R.; Haque, F. Z.; Kurchania, R. Effects of annealing temperature optimization on the efficiency of ZnO nanoparticles photoanode based dye sensitized solar cells. *J. Mater. Sci. Mater. Electron.* **2017**, *28*, 1537–1545. https://doi.org/10.1007/s10854-016-5693-9.

(65) Khan, A. Raman Spectroscopic Study of the ZnO Nanostructures. *J. Pakistan Mater. Soc.* **2010**, *4*, 5–9. http://mrl.uop.edu.pk/JPMS/issues/jpms7/5-9 Raman Spectroscopic Study of the ZnO Nanostructures Aurangzeb Khan.pdf.

(66) Li, H.; Ban, L.; Niu, Z.; Huang, X.; Meng, P.; Han, X.; Zhang, Y.; Zhang, H.; Zhao, Y. Application of Cu_xO-Fe_yO_z nanocatalysts in ethynylation of formaldehyde. *Nanomaterials.* **2019**, *9*, 1–15. https://doi.org/10.3390/nano9091301.

(67) Munoz-Munoz, Y. M.; Guevara-Carrion, G.; Vrabec, J. Molecular Insight into the Liquid Propan-2-ol + Water Mixture. *J. Phys. Chem. B.* **2018**, *122*, 8718–8729. https://doi.org/10.1021/acs.jpcb.8b05610.

(68) Crupi, V.; Majolino, D.; Migliardo, P.; Venuti, V. Inter- and intramolecular hydrogen bond in liquid polymers: A Fourier transform infrared response. *Mol. Phys.* **2000**, *98*, 1589–1594. https://doi.org/10.1080/00268970009483364.

(69) Daira, R.; Kabir, A.; Boudjema, B.; Sedrati, C. Structural and optical transmittance analysis of CuO thin films deposited by the spray pyrolysis method. *Solid State Sci.* **2020**, *104*, 106254. https://doi.org/10.1016/j.solidstatesciences.2020.106254.